Document Number
TRACOR 65-292-U

Technical Memorandum

AN IMPROVED ANALYTICAL MODEL OF THE INTERACTION OF DOMES AND TRANSDUCERS DURING TRANSMISSION

Prepared for the

Bureau of Ships
Code 1622E

Contract NObsr 91229
Project Number SF 00103, Task 8139
August 31 1965

TRACOR INC
1701 GUADALUPE ST. AUSTIN TEXAS 78701 GR6-6601

Document Number
TRACOR 65-292-U

TRACOR, INC 1701 Guadalupe St Austin, Texas 78701

Technical Memorandum

AN IMPROVED ANALYTICAL MODEL OF THE INTERACTION OF DOMES AND TRANSDUCERS DURING TRANSMISSION

Prepared for the

Bureau of Ships
Code 1622E

Contract NObsr 91229
Project Number SF 00103, Task 8139
August 31, 1965

Prepared By:

W. C. Moyer

J. D. Morell

Karolen Glass

TABLE OF CONTENTS

TRACOR, INC 1701 Guadalupe St Austin, Texas 78701

AN IMPROVED ANALYTICAL MODEL OF THE INTERACTION OF DOMES AND TRANSDUCERS DURING TRANSMISSION

I. INTRODUCTION

The purpose of this technical memorandum is to describe an improvement in the specification of transducer velocity distributions which are used in the analysis of dome-transducer interactions. The mathematical model used in these studies consists of a circular cylinder and concentric shell. Typically the interaction problem has been studied by obtaining a solution to the boundary value problem defined by the geometry of the cylinder and concentric shell.

In previous studies[1] a velocity equivalent to the radial component of a plane sound pressure wave has been specified on a portion of the cylinder face, the remainder of the cylinder being rigid. The portion of the cylinder face having nonzero velocity represents the active elements of the transducer. For such a velocity specification, the velocity (amplitude and phase) is continuous across the active face. This specification is somewhat fictitious since it is equivalent to an infinite number of point sources. In a real transducer there are, of course, a finite number of active elements having finite dimensions and discrete velocity amplitudes and phases.

Recently, a computational procedure has been developed which permits the active portion of the cylinder face to be separated into finite segments, each of which has a discrete velocity amplitude and phase. The mathematical form of the function describing the velocity boundary condition specified on the cylinder has a finite number of finite discontinuities as compared to the previous continuous description. This new boundary specification is clearly a more realistic one.

One important result of the improved boundary specification is that dome-transducer interactions now can be analyzed for various transducer element shading and phasing factors. This generality, not available in previous boundary specifications, will permit the investigation of an "optimum" element shading and phasing including the effects of the dome.

In addition to the mathematical details of the new boundary specification, some computed results for the near- and farfields of the dome-transducer are included in this memorandum. These results are compared with results previously obtained for a continuous velocity distribution. Results are also presented for several types of shading to indicate dome effects on the nearfield sound pressure distribution and on beamwidth and side lobe suppression as a function of transducer shading.

II. FORMULATION

The interaction of the dome and transducer is analyzed by obtaining a solution to the scalar wave equation for boundary conditions prescribed on the transducer and dome surfaces. The geometry of the dome-transducer model considered in this memorandum is identical to the geometry considered in previous studies (see Ref. 1) and is shown in Fig. 1.

The boundary conditions typically employed in the boundary value problem are that the normal particle velocity of the fluid have a prescribed value at the transducer face and that the normal particle velocity be continuous at the shell-fluid interfaces. In previous studies the normal particle velocity specified on the active portion of the transducer face was equal to the radial component of the particle velocity of a plane pressure wave, the remainder of the cylinder being rigid. This boundary condition has the mathematical representation *

$$v|_{r=a} = \cos\theta \; e^{ika\cos} \qquad 0 < |\theta| < \varphi$$
$$= 0 \qquad \varphi < |\theta| < \pi \quad . \tag{1}$$

where

v is the particle velocity of the fluid normal to the transducer.,

$k = \frac{2\pi}{\lambda}$ and λ is the wavelength of the transmitted wave,

and a is the radius of the transducer.

*The time component $e^{-i\omega t}$, where ω is the angular frequency, will be suppressed.

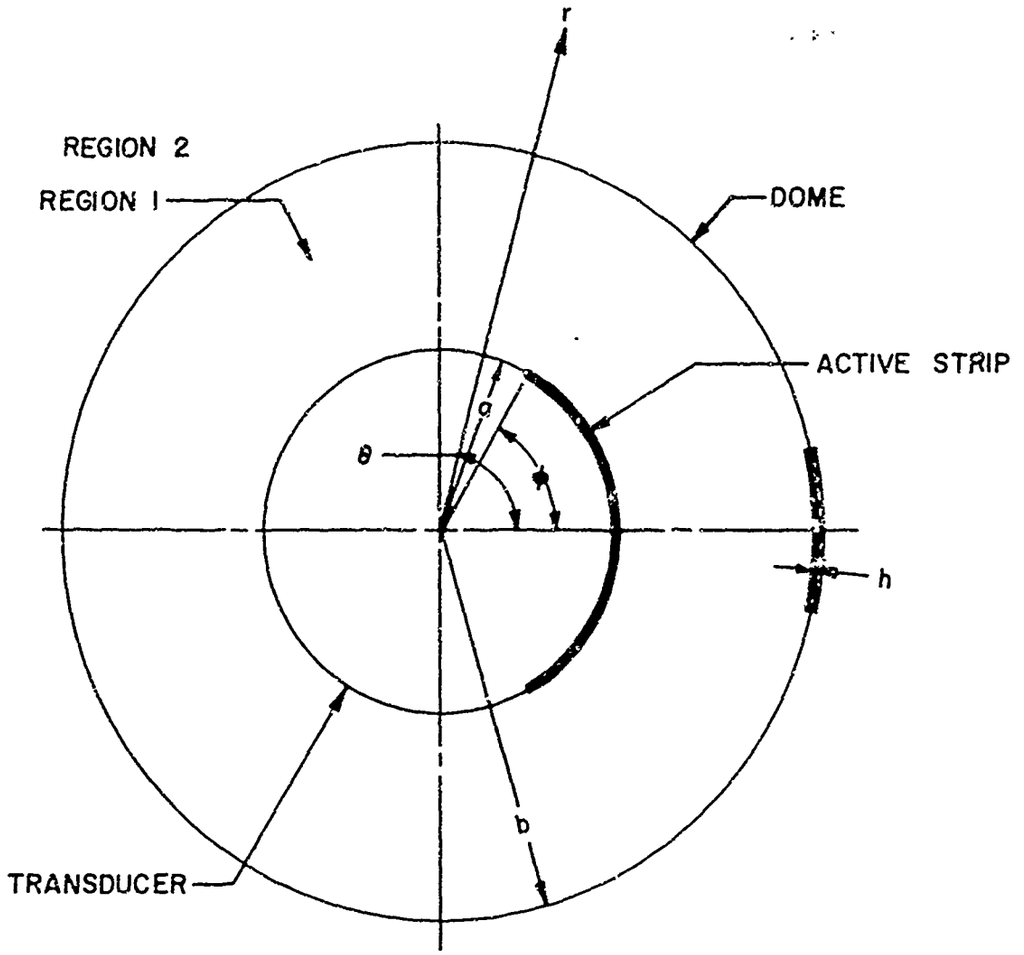

FIG. 1 - GEOMETRY FOR A CYLINDRICAL TRANSDUCER RADIATING IN A CONCENTRIC DOME

TRACOR, 1 DWG. 778-1
AUSTIN, TEXAS 3/19/65 BM/LRH

This boundary representation has the effect of shading each point on the active portion of the boundary by a cos θ factor and phasing each point to a straight line. In this memorandum a velocity condition is employed having the representation

$$v|_{r=a} = \{V_j\} \quad , \tag{2}$$

where

$\{V_j\}$ is the set of head velocities of the active transducer elements, and V_j is the complex normal velocity of the jth element in the transducer.

It is assumed that the new velocity specification is an even function of θ although other cases can be handled with little increase in difficulty. A comparison of the continuous and discrete boundary conditions is shown graphically in Fig. 2

The velocity of any particular active element in the transducer array can be written as

$$V_j = |V_j| e^{i\varphi_j} \tag{3}$$

where $|V_j|$ is the velocity amplitude and φ_j is the phase of the jth element.

The velocity specification for a single element of width 2β and angular position $\gamma=(2j-1)\alpha$ as shown in Fig. 3 is

$$\begin{aligned} v|_{r=a} &= 0 && 0 < |\theta| < \gamma - \beta \\ &= |V_j| e^{i\varphi_j} && \gamma-\beta<|\theta| < \gamma + \beta \\ &= 0 && \gamma+\beta<|\theta| < \pi \end{aligned} \tag{4}$$

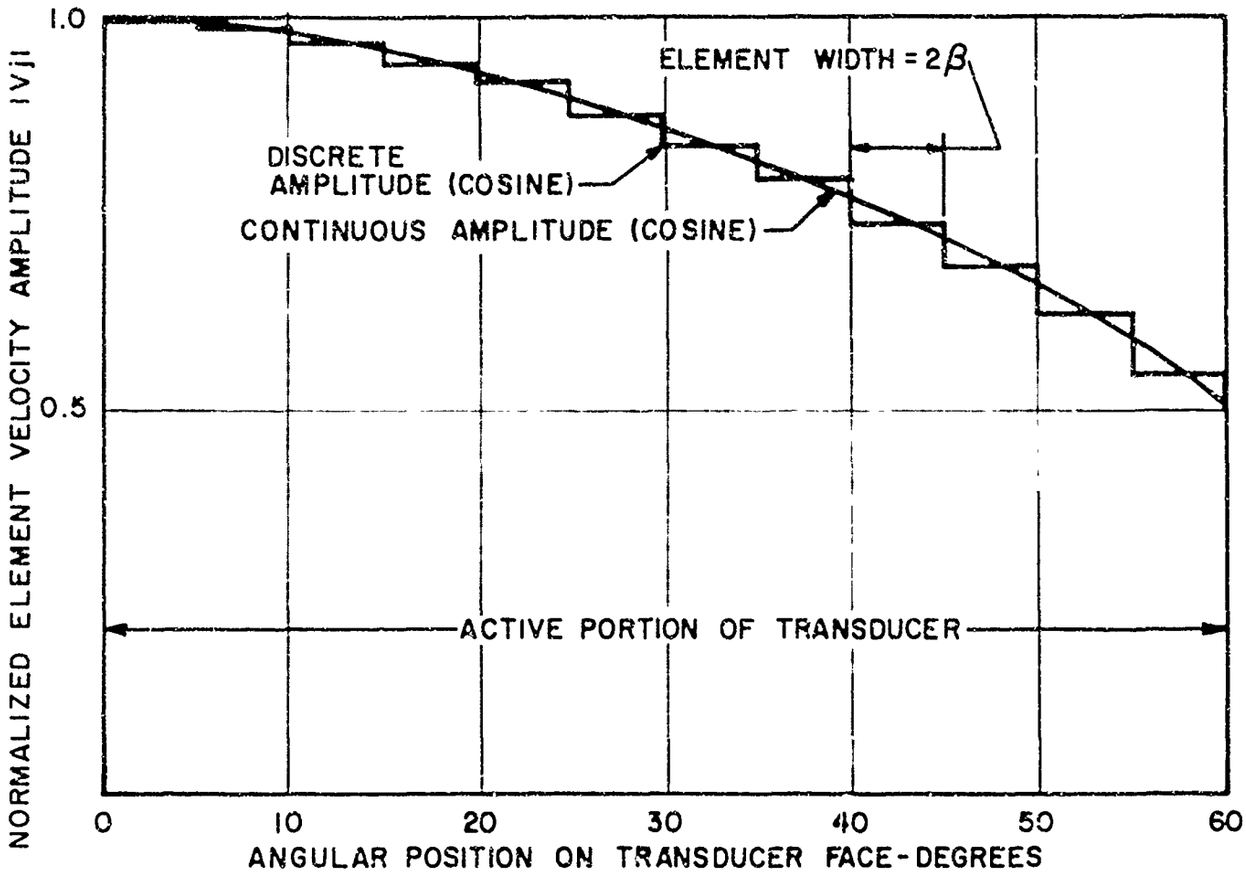

FIG. 2 -CONTINUOUS AND DISCRETE BOUNDARY CONDITIONS PRESCRIBED FOR THE DOME-TRANSDUCER MODEL

TRACOR, INC | DWG 778-64
AUSTIN, TEXAS 8/27/65 BM/LBH

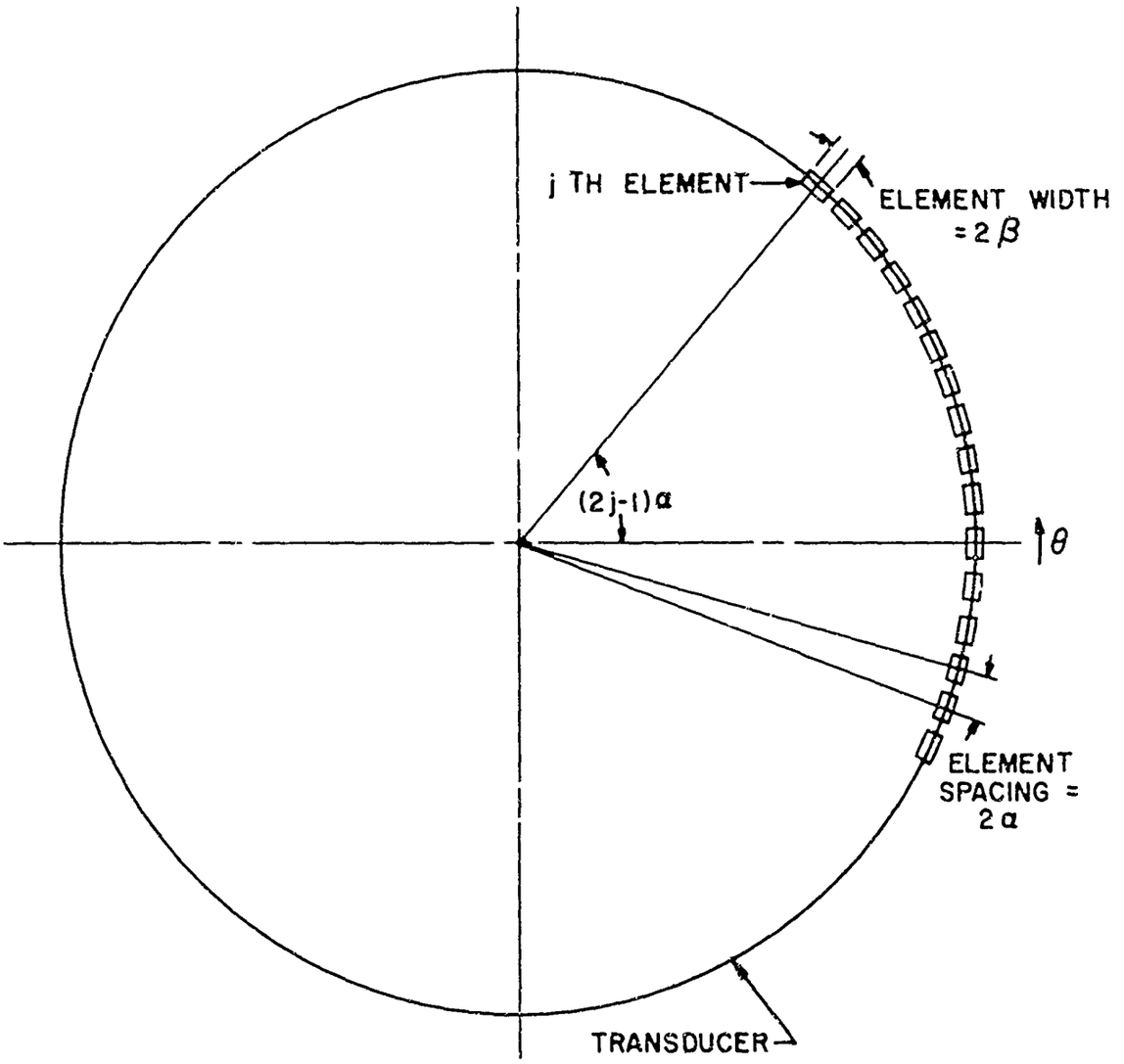

FIG. 3 - TRANSDUCER ELEMENT GEOMETRY

MAJOR, INC | DWG 778-63
AUSTIN, TEXAS 8/27/65 BM/LBH

This distribution has a Fourier Series representation

$$v|_{r=a} = \sum_{n=0}^{\infty} \delta_n \cos n\theta \tag{5}$$

where

$$\begin{aligned}\delta_n &= \frac{\varepsilon_n}{\pi} \int_{\gamma-\beta}^{\gamma+\beta} |V| e^{i\varphi} \cos n\theta d\theta \\ &= \frac{2\beta}{\pi} |V| e^{i\varphi} \quad , \quad n=0 \\ &= \frac{2}{n\pi} |V| e^{i\varphi} [\sin n(\gamma+\beta) - \sin n(\gamma-\beta)], \\ &\qquad\qquad\qquad\qquad\qquad\qquad n>0 \ ,\end{aligned}$$

and $\varepsilon_n = 1$ for $n = 0$, $\varepsilon_n = 2$ for $n>0$.

Since the problem is linear, the velocity distribution for several elements can be obtained by vector addition of the velocities of individual elements. Thus if an array of 2N equally-spaced, active elements is chosen as shown in Fig. 3, with the jth element having a velocity given by Eq. 3, the boundary condition takes the form

$$\begin{aligned}V|_{r=a} &= V_1 e^{i\varphi_1} && \alpha-\beta<|\theta|<\alpha+\beta \\ &= V_2 e^{i\varphi_2} && 3\alpha-\beta<|\theta|<3\alpha+\beta \\ &\ \ \vdots \\ &= V_j e^{i\varphi_j} && (2j-1)\alpha-\beta<|\theta|<(2j-1)\alpha+\beta \\ &\ \ \vdots \\ &= V_N e^{i\varphi_N} && (2N-1)\alpha-\beta<|\theta|<(2N-1)\alpha+\beta \\ &= 0 && \text{elsewhere}\end{aligned} \tag{6}$$

where 2α is the element spacing and 2β is the element face width.

In a manner analogous to Eq. 5, Eq. 6 can be given a Fourier series representation

$$v|_{r=a} = \sum_{n=0}^{\infty} \delta_n \cos n\theta \qquad (7)$$

where

$$\delta_n = \frac{2\beta}{\pi} \sum_{j=1}^{N} |V_j| e^{i\varphi_j} \ , \ n=0$$

and

$$\delta_n = \frac{2}{n\pi} \sum_{j=1}^{N} |V_j| e^{i\varphi_j} \{\sin n[(2j-1)\alpha+\beta]$$

$$- \sin n[(2j-1)\alpha-\beta]\} \ , \ n>0.$$

The boundary condition is now in a form suitable for use in determining the sound pressure field inside and outside the dome.

The mathematical details of solving the boundary value problem for a continuous boundary condition are given in Appendix A. The solution of a boundary value problem having a boundary condition given by Eq. 7 is obtained in exactly the same manner by substituting Eq. 7 for Eq. 9, Appendix A, and carrying out the indicated operations in Appendix A.

III. NUMERICAL RESULTS

Numerical results were computed for the sound pressure in the near- and farfields of the transducer in order to determine the effect of the dome on transmitted beams. Results were obtained for several sets of amplitude shading factors $|V_j|$ as given in Eq. 6. For all computed results, the phasing factors φ_j, given in Eq. 6, were chosen so that the elements were phased to a straight line. The results were computed for parameters appropriate to the AN/SQS-26. Results with and without the dome are presented. In each case the results are normalized to the maximum sound pressure in the distribution.

The near- and farfield pressure distributions for a transducer having unity shading factors are given in Figs. 4 and 5.* The near- and farfield pressure sound pressures presented in Figs. 6 and 7 are for amplitude shading factors having a cosine distribution. For this case the amplitude factor $|V_j|$ is obtained as

$$|V_j| = \cos\,(2j-1)\alpha \quad . \tag{8}$$

A comparison of the near- and farfields obtained with continuous and discrete transducer velocity distributions is given in the linear plots of Figs. 8, 9, 10, and 11. The former results, which have continuous phasing and shading (cosine), were obtained from Ref. 1.

*For the results presented, the transducer radius is a, the dome radius is b, the dome thickness is h (h=0 indicates no dome is present), and r is the radial distance from the center of the transducer at which the sound pressure field was computed. All dimensions are in inches.

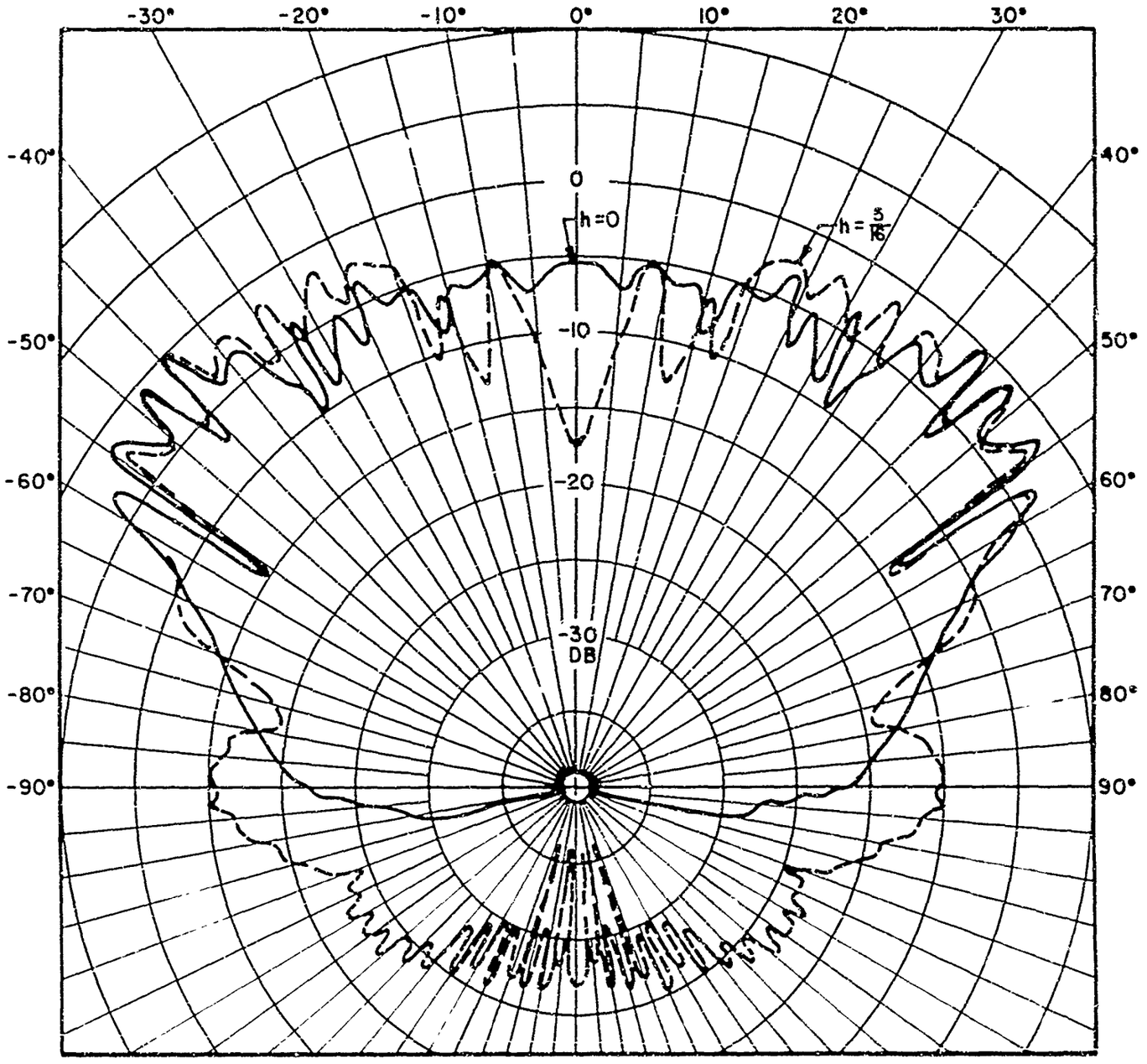

FIG. 4 -SOUND PRESSURE DISTRIBUTION (DB) FOR A TRANSDUCER RADIATING INSIDE A CONCENTRIC DOME

a = 96 b=120 r=96

SHADING = UNITY

TRACOR, INC 1 DWG. 778-56
AUSTIN, TEXAS 8/23/65 BM/LBH

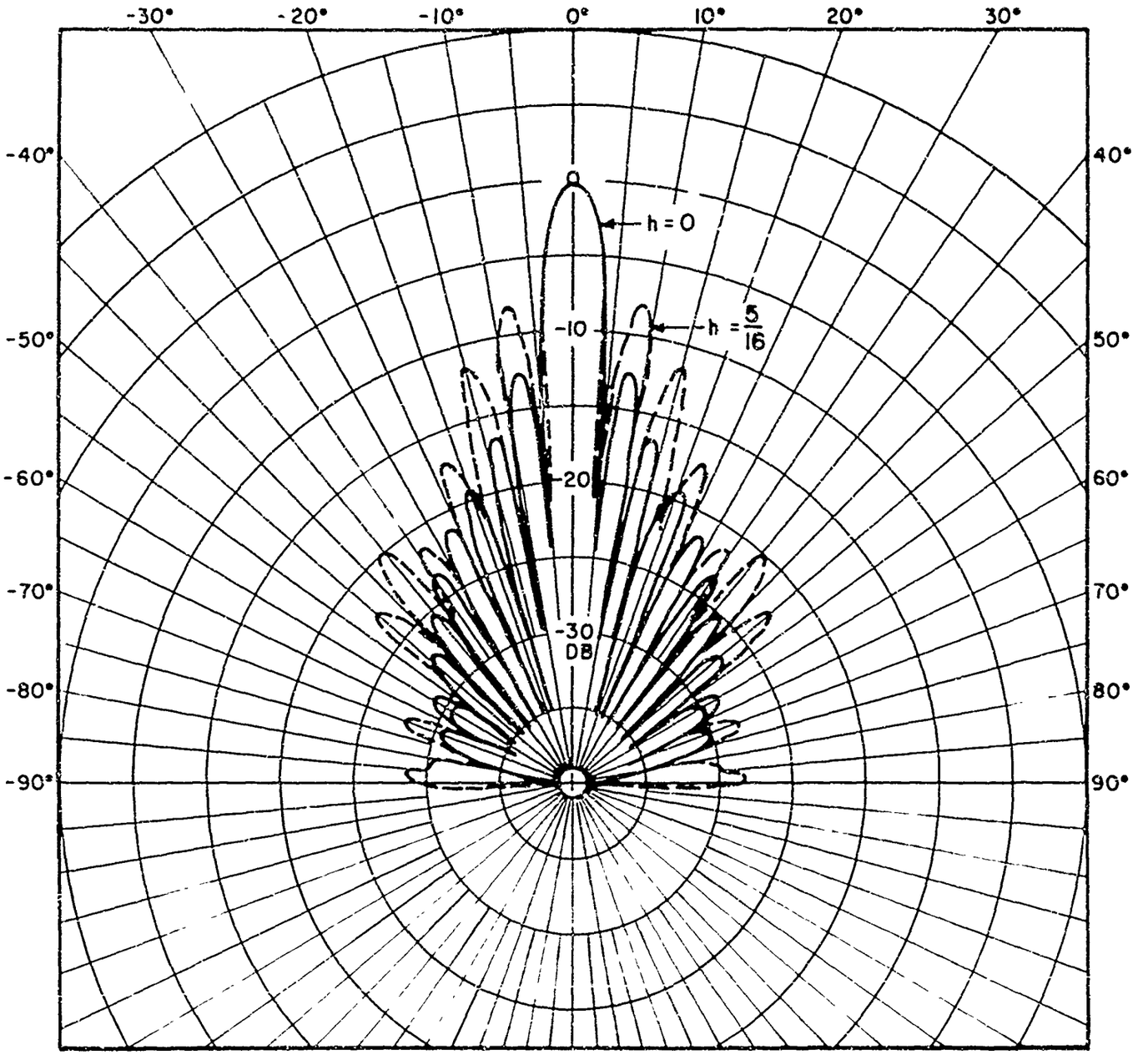

FIG. 5 - SOUND PRESSURE DISTRIBUTION (DB) FOR A TRANSDUCER RADIATING INSIDE A CONCENTRIC DOME

a = 96 b= 120 r = FARFIELD

SHADING = UNITY

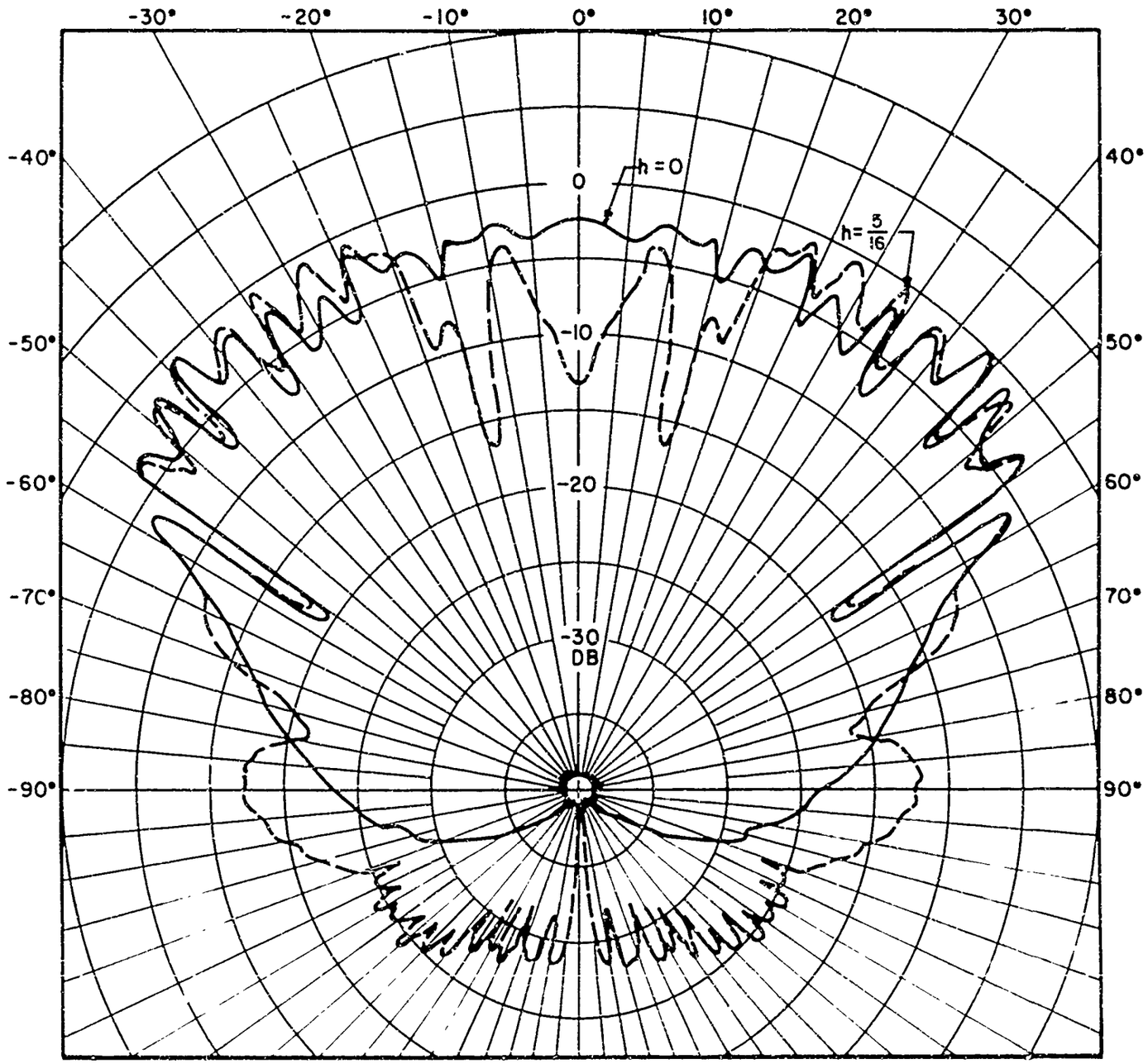

FIG. 6 -SOUND PRESSURE DISTRIBUTION (DB) FOR A TRANSDUCER RADIATING INSIDE A CONCENTRIC DOME

a = 96 b = 120 r = 96

SHADING = COSINE

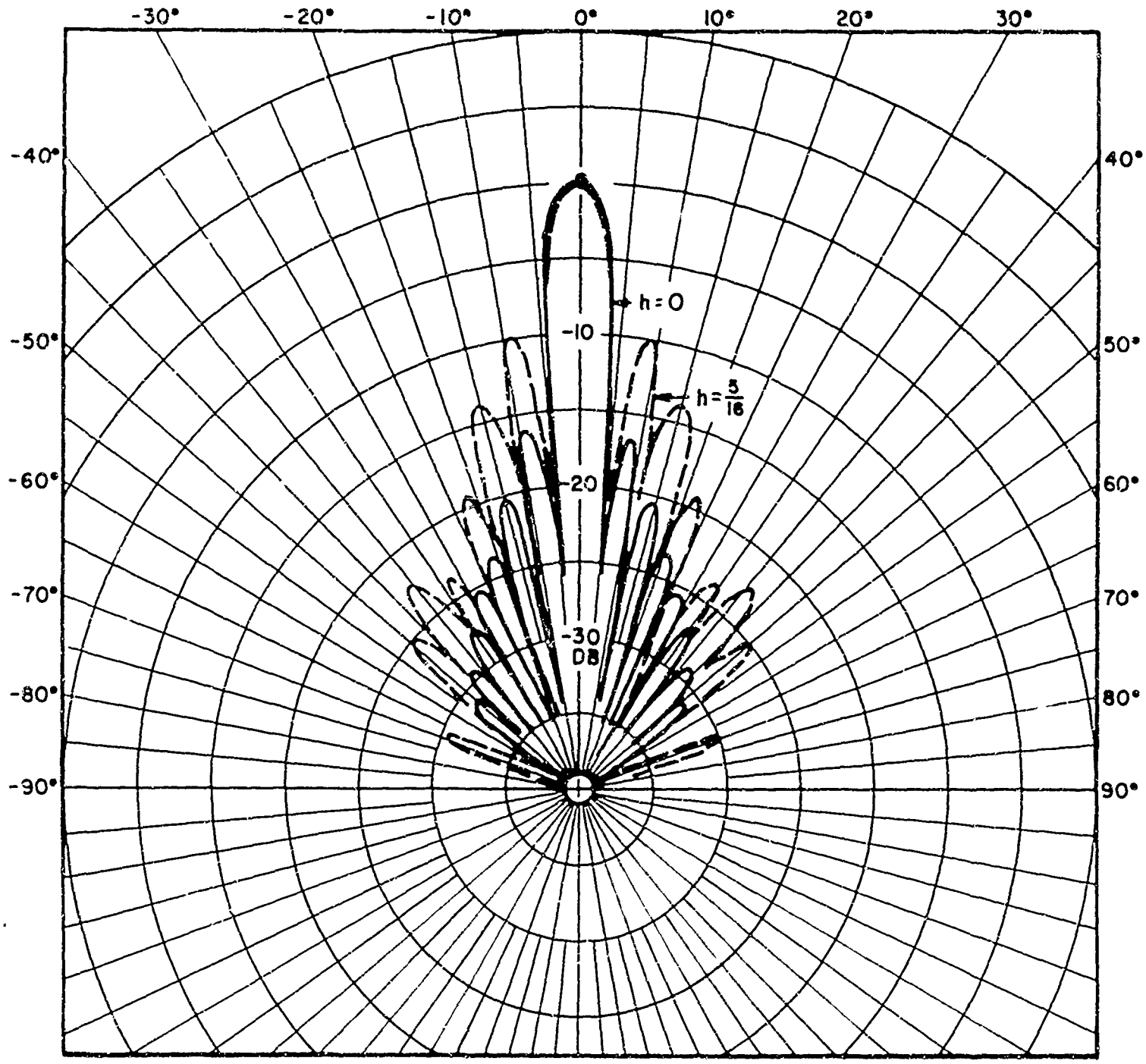

FIG. 7 -SOUND PRESSURE DISTRIBUTION (DB) FOR A TRANSDUCER RADIATING INSIDE A CONCENTRIC DOME

a = 96 b = 120 r = FARFIELD

SHADING = COSINE

TRACOR, INC | DWG. 778-45

AUSTIN, TEXAS 8/23/66 BM/LBH

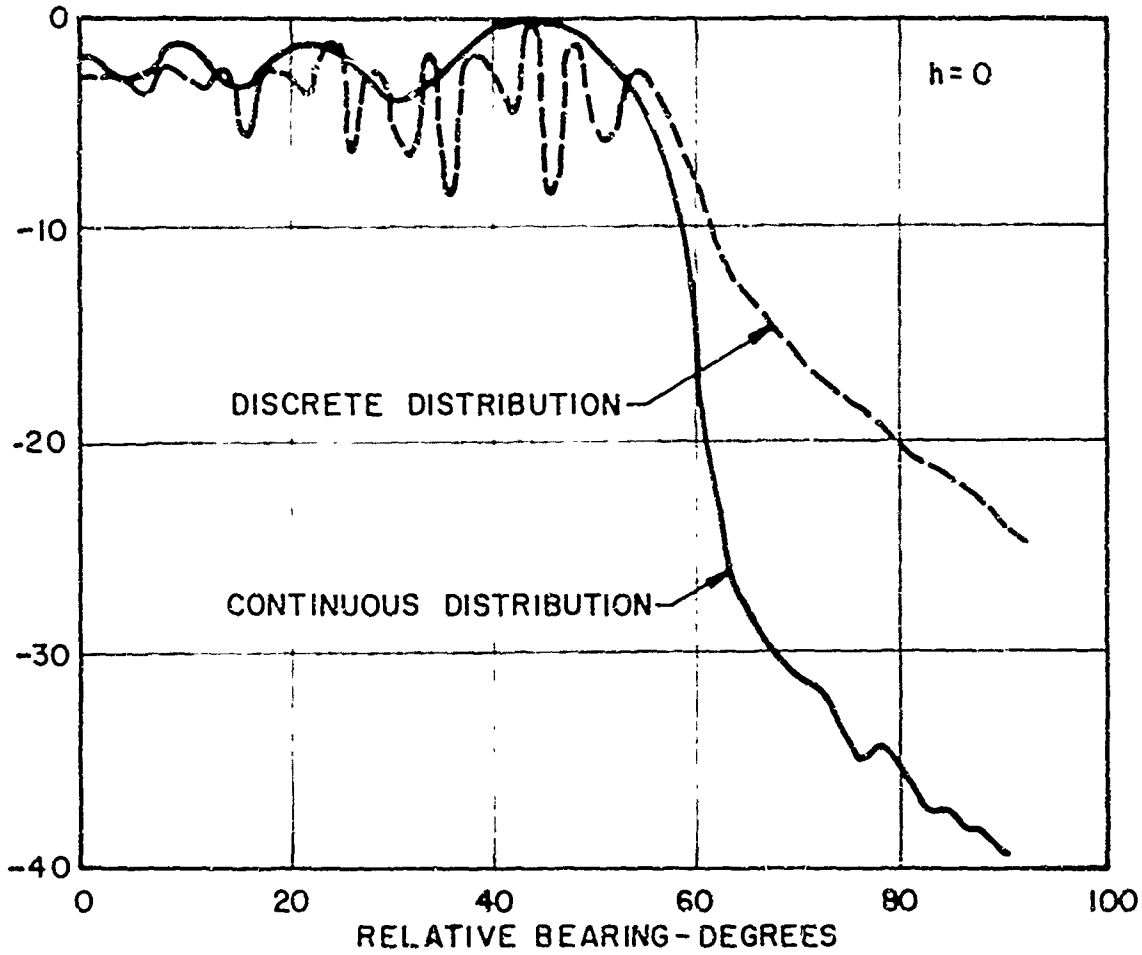

FIG. 8 -SOUND PRESSURE DISTRIBUTION (DB) FOR A TRANSDUCER RADIATING INSIDE A CONCENTRIC DOME

a = 96 b = 120 r = 96

SHADING = COSINE

TRACOR, INC | DWG 778-49
AUSTIN, TEXAS 8/23/66 BM/LBH

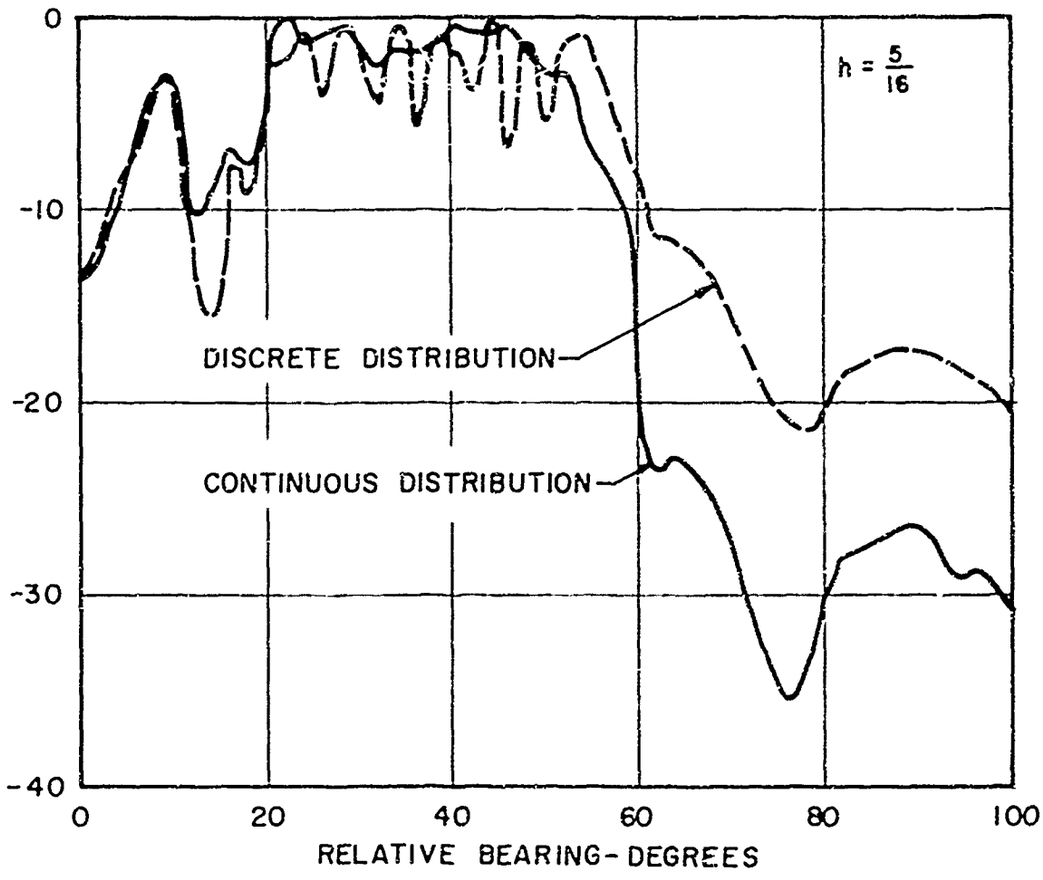

FIG. 9 -SOUND PRESSURE DISTRIBUTION (DB) FOR A TRANSDUCER RADIATING INSIDE A CONCENTRIC DOME

a = 96 b=120 r= 96

SHADING = COSINE

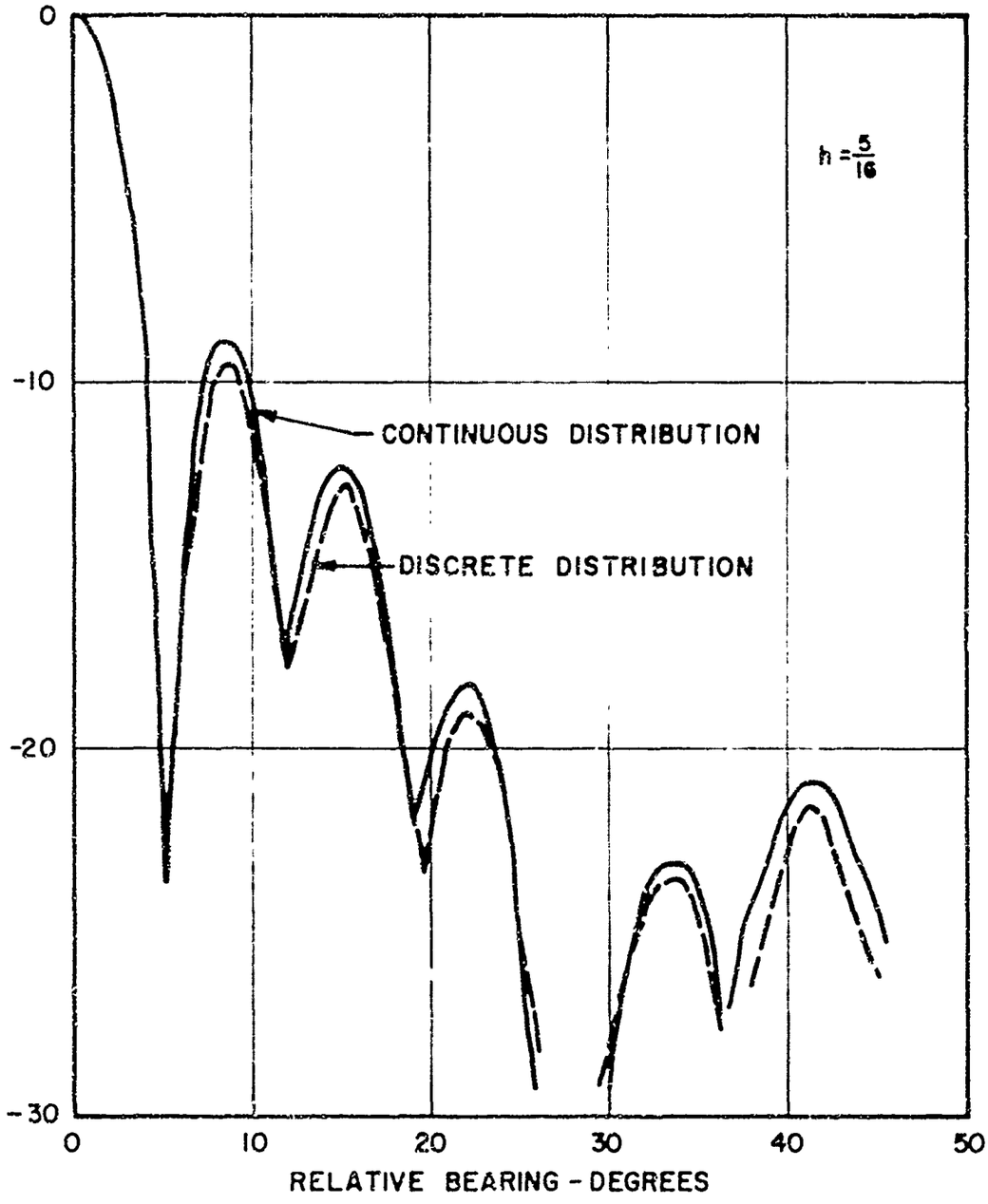

FIG. 10 -SOUND PRESSURE DISTRIBUTION (DB) FOR A TRANSDUCER RADIATING INSIDE A CONCENTRIC DOME

a = 96 b = 120 r = FARFIELD

SHADING = COSINE

TRACOR, INC | DWG. 778-51
AUSTIN, TEXAS 6/23/65 BM/LBH

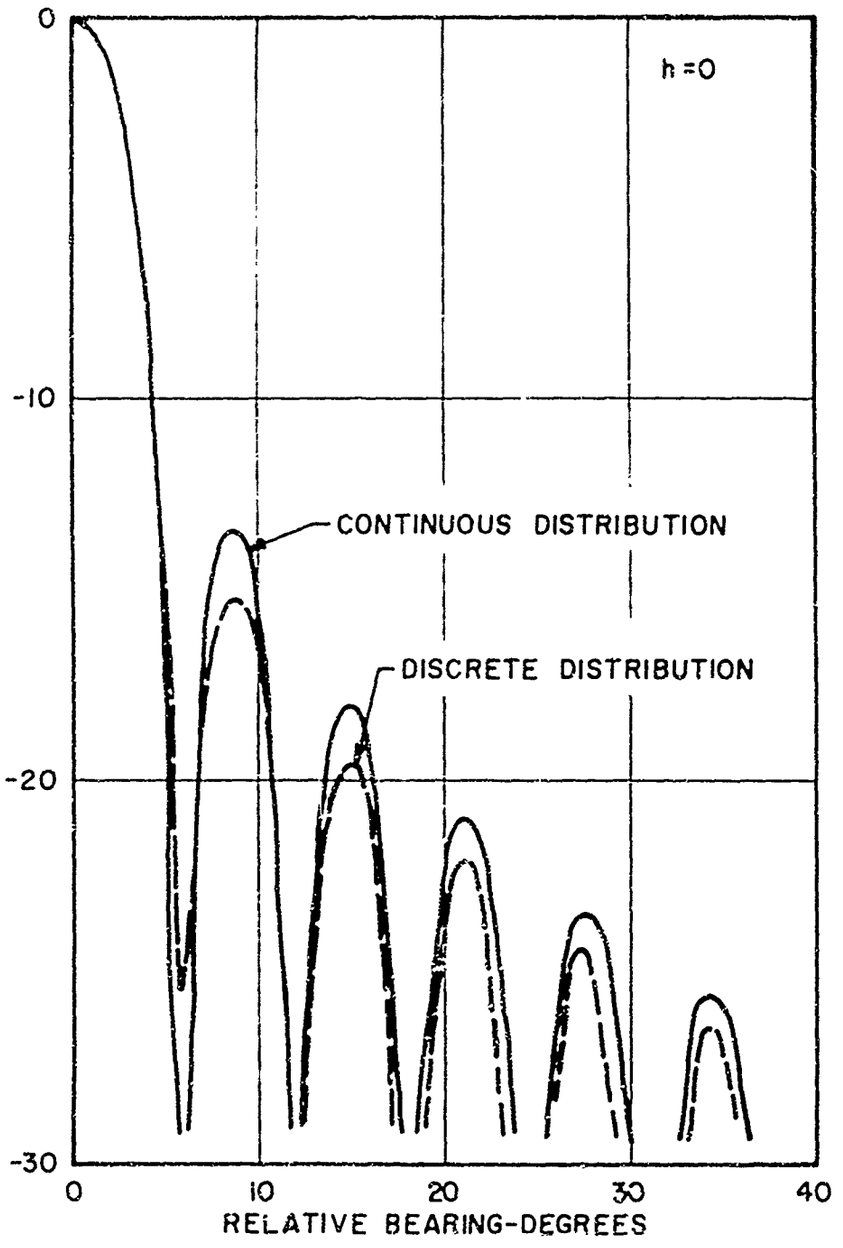

FIG. 11 -SOUND PRESSURE DISTRIBUTION (DB) FOR A TRANSDUCER RADIATING INSIDE A CONCENTRIC DOME

a = 96 b = 120 r = FARFIELD

SHADING = COSINE

TRACOR, INC | DWG 778-52
AUSTIN, TEXAS 8/23/66 BM/LBH

Results for amplitude shading factors which have a cosine-squared distribution, i.e.,

$$|V_j| = \cos^2(2j-1)\alpha \quad , \tag{9}$$

are given in Figs. 12 and 13. Shading factors corresponding to those for the AN/SQS-26, Model XN-2, were used to compute the results shown in Figs. 14 and 15. Finally, shading factors derived by the method of Dolph-Tchebyscheff[2] were used in obtaining the results shown in Figs. 16 and 17.

A compilation of the shading factors is given in Table 1.

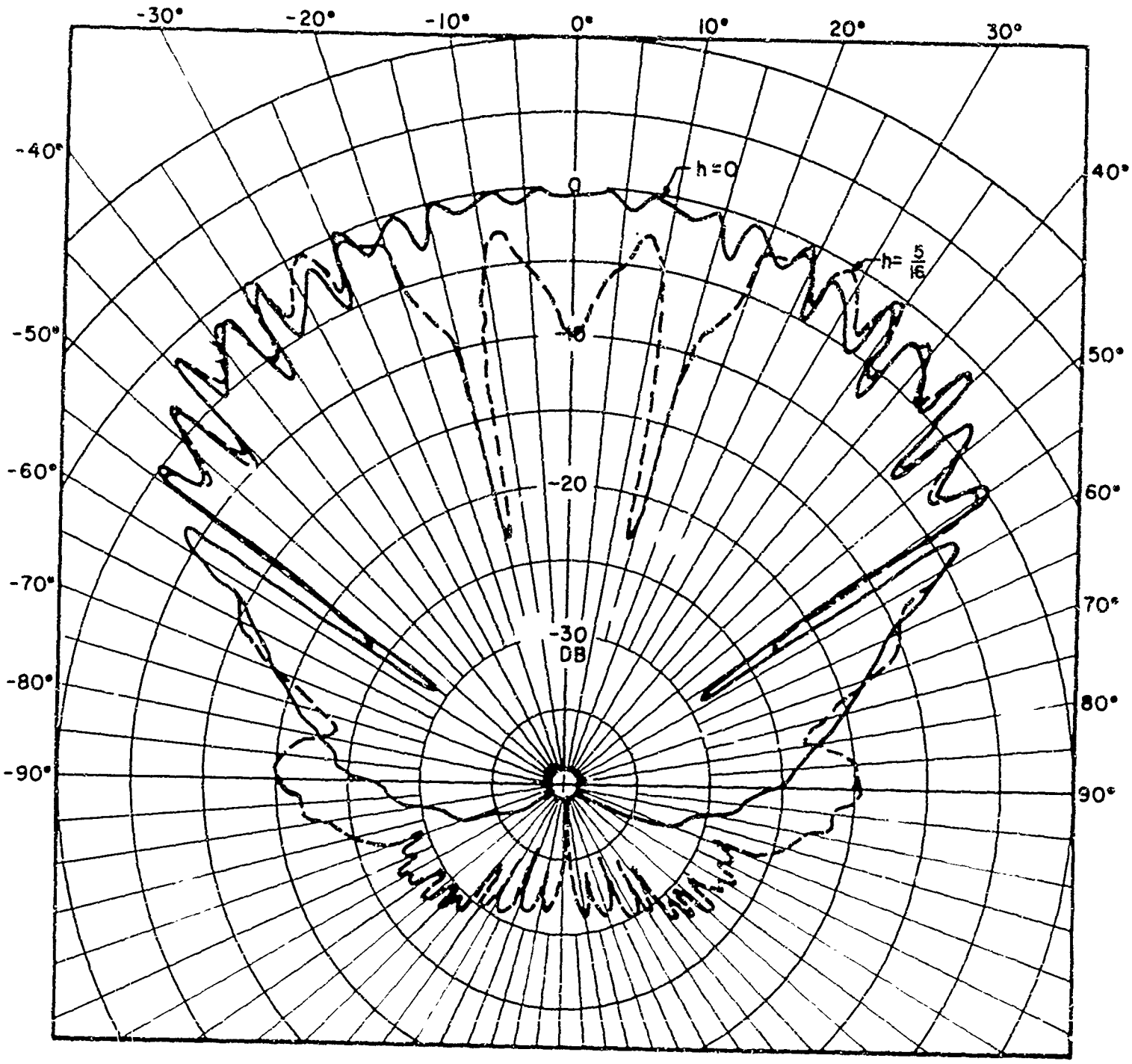

FIG. 12 -SOUND PRESSURE DISTRIBUTION (DB) FOR A TRANSDUCER RADIATING INSIDE A CONCENTRIC DOME

a = 96 b= 120 r = 96

SHADING = COSINE ^{2}

TRACOR, INC | DWG. 778-53

AUSTIN, TEXAS 8/23/66 BM/LBH

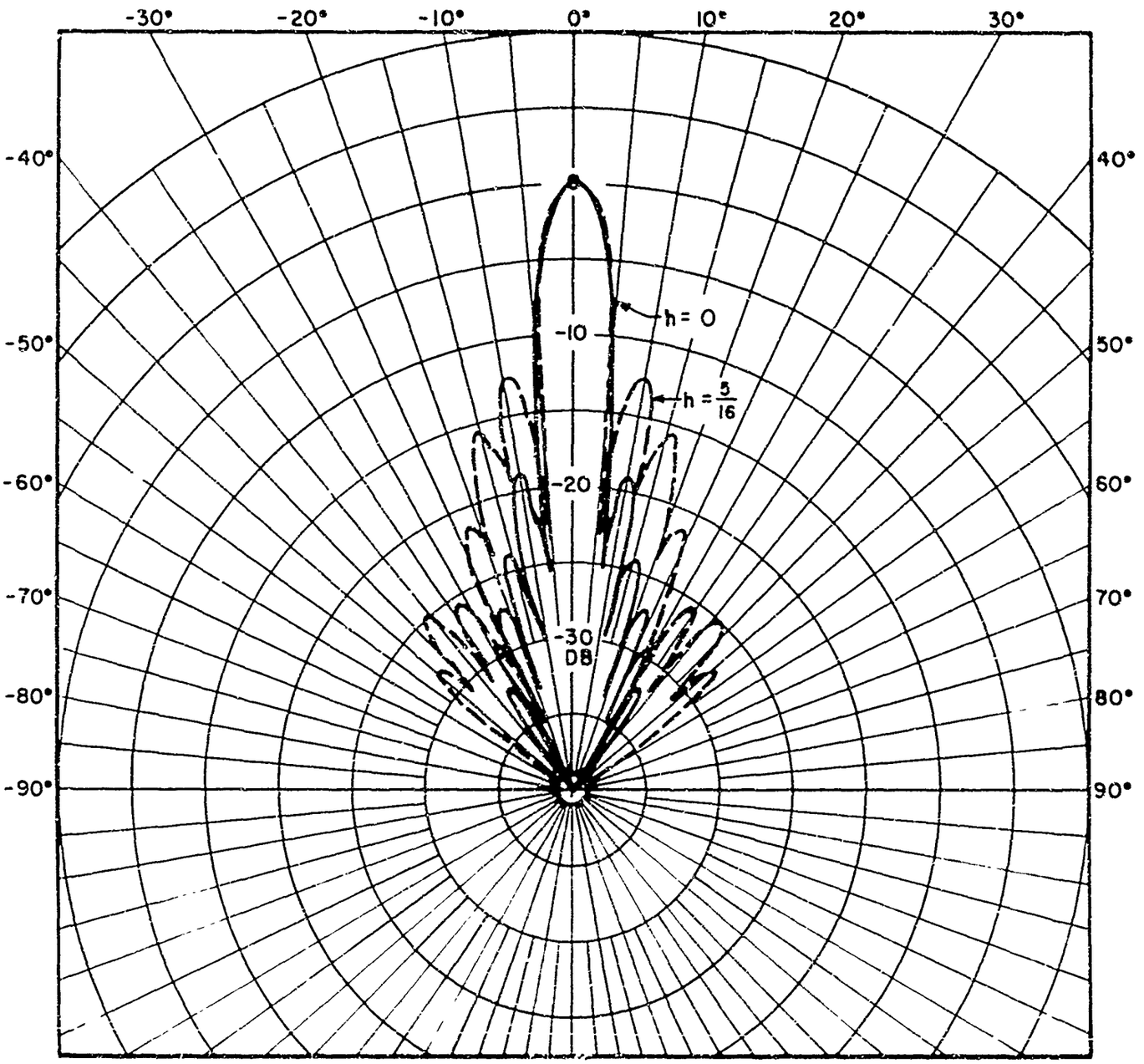

FIG. 13 -SOUND PRESSURE DISTRIBUTION (DB) FOR A TRANSDUCER RADIATING INSIDE A CONCENTRIC DOME

a = 96 b = 120 r = FARFIELD

SHADING = COSINE ^{2}

TRACOR, INC | DWG. 778-46
AUSTIN, TEXAS 8/23/65 BM/LEH

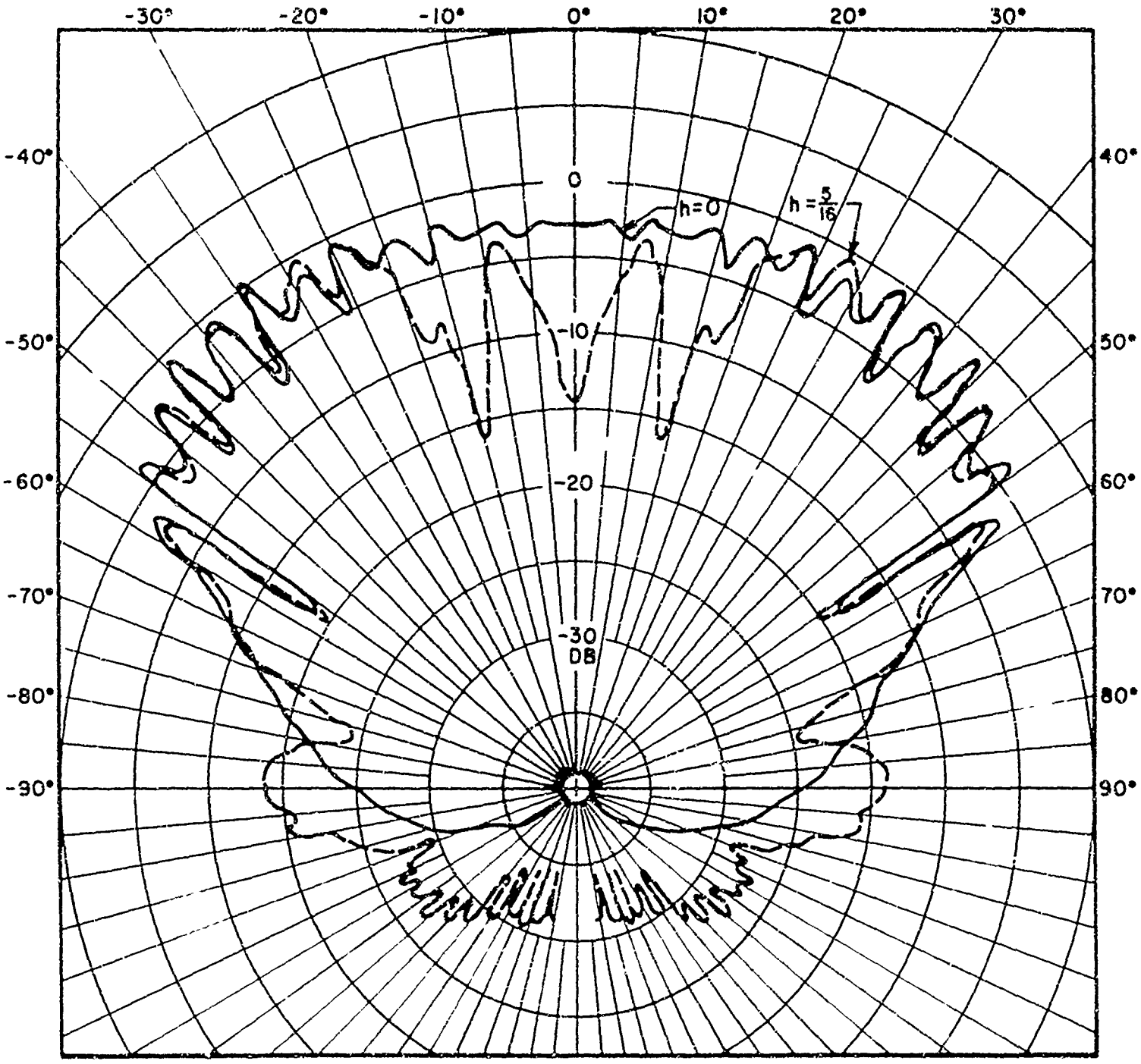

FIG. 14 -SOUND PRESSURE DISTRIBUTION (DB) FOR A TRANSDUCER RADIATING INSIDE A CONCENTRIC DOME

a = 96 b= 120 r=96

SHADING = AN/SQS-26, XN-2

TRACOR, INC | DWG. 776-55

AUSTIN, TEXAS 8/23/68 BM/LBM

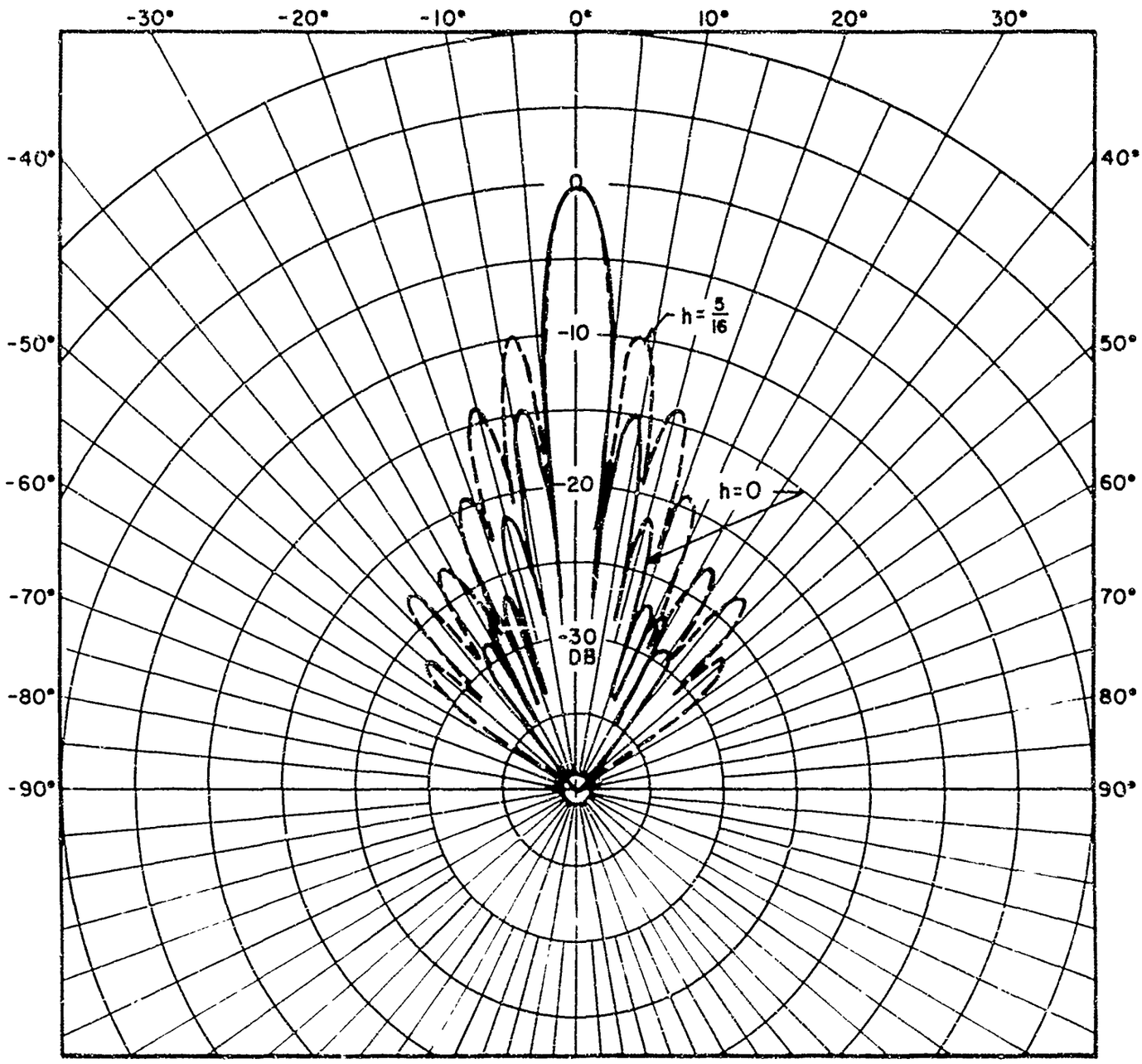

FIG. 15 -SOUND PRESSURE DISTRIBUTION (DB) FOR A TRANSDUCER RADIATING INSIDE A CONCENTRIC DOME

a = 96 b= 120 r = FARFIELD

SHADING = AN/SQS 26 , XN2

TRACOR, INC | DWG. 778-47
AUSTIN, TEXAS 8/23/65 BM / LBH

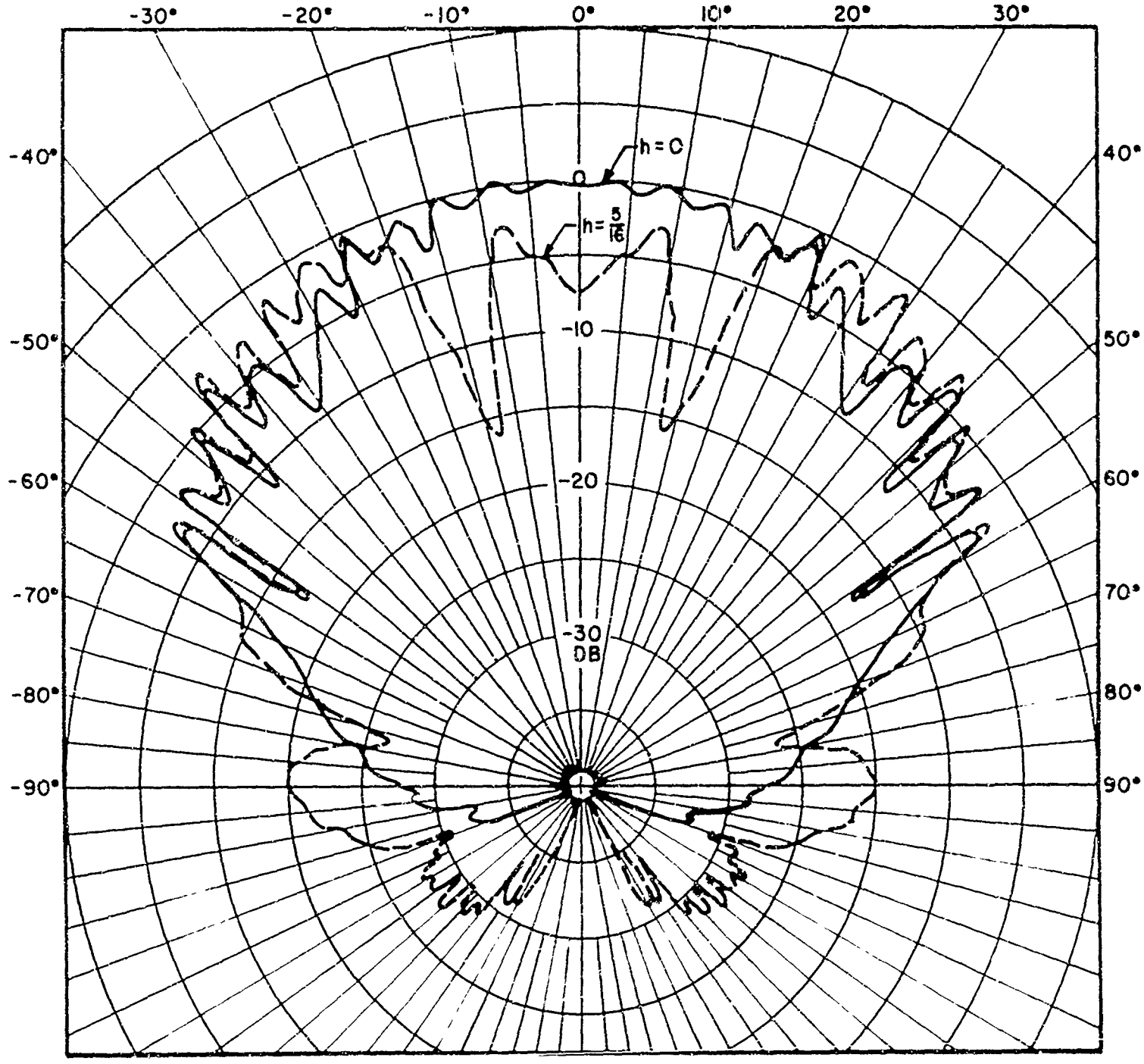

FIG. 16 -SOUND PRESSURE DISTRIBUTION (DB) FOR A TRANSDUCER RADIATING INSIDE A CONCENTRIC DOME

a = 96 b= 120 r = 96

SHADING = DOLPH-TCHEBYSCHEFF

TRACOR, INC | DWG. 778-54

AUSTIN, TEXAS 8/23/68 BM/LBH

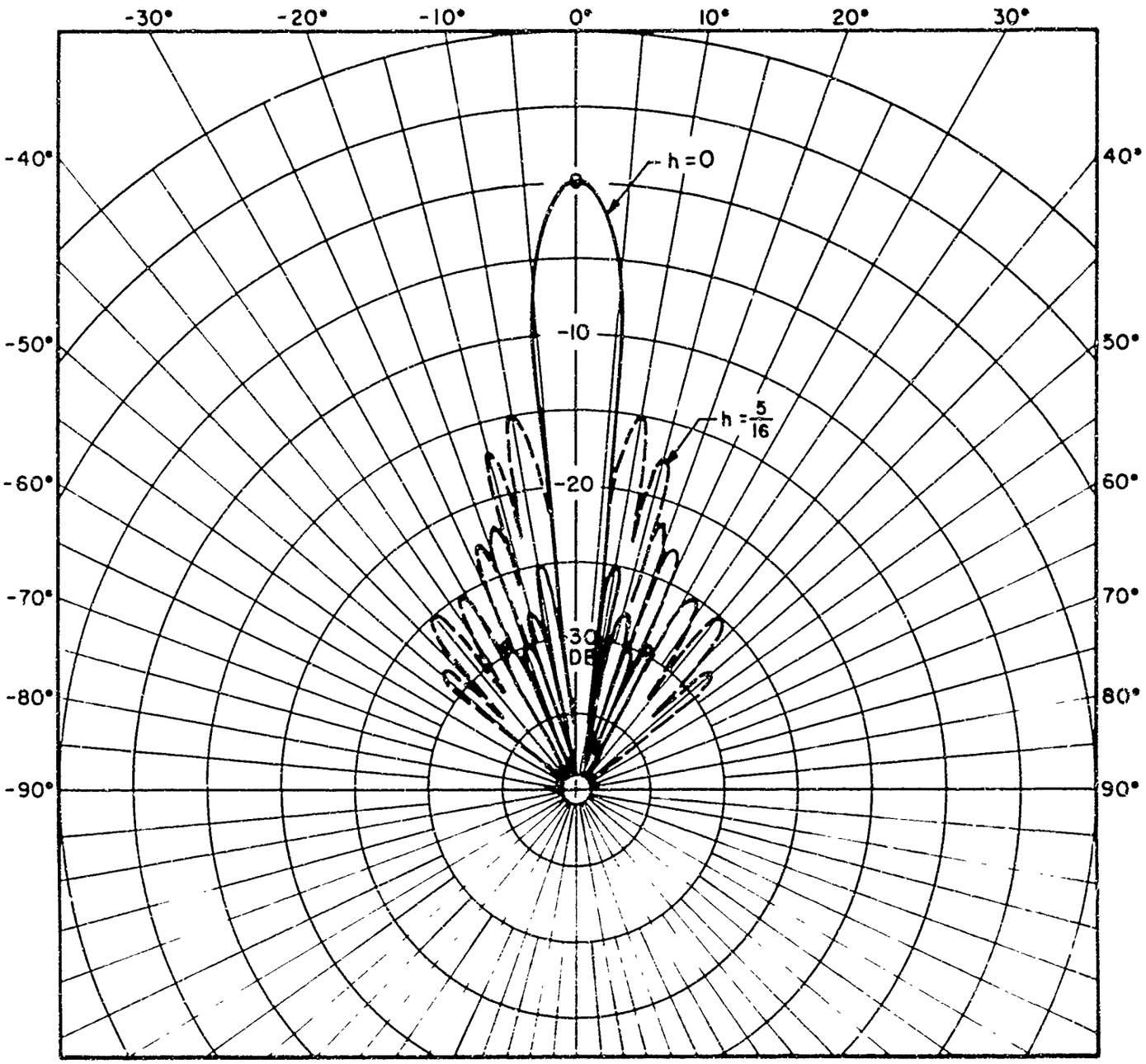

FIG. 17 -SOUND PRESSURE DISTRIBUTION (DB) FOR A TRANSDUCER RADIATING INSIDE A CONCENTRIC DOME

a = 96 b = 120 r = FARFIELD

SHADING = DOLPH-TCHEBYSCHEFF

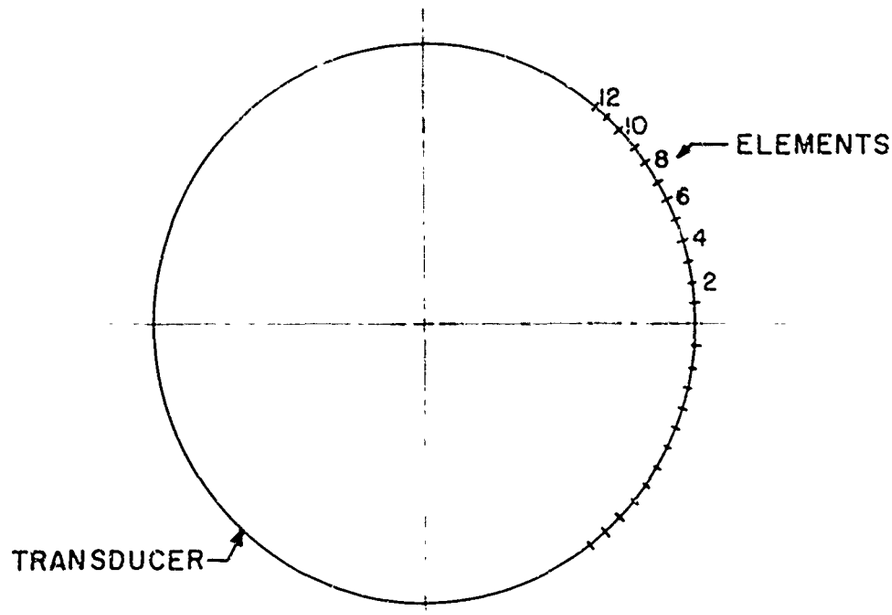

SHADING FACTORS $|V_j|$

	SHADING TYPE				
ELEMENT NO.	UNITY	COSINE	COS^2	XN-2	DOLPH
1	1.00	.999	.999	1.00	1.00
2	1.00	.991	.982	1.00	.980
3	1.00	.976	.953	1.00	.925
4	1.00	.954	.910	1.00	.850
5	1.00	.924	.854	1.00	.760
6	1.00	.887	.787	1.00	.665
7	1.00	.843	.711	1.00	.570
8	1.00	.793	.629	.933	.475
9	1.00	.737	.543	.708	.390
10	1.00	.676	.457	.631	.315
11	1.00	.609	.371	.562	.265
12	1.00	.537	.288	.501	.315

TABLE I - ELEMENT AMPLITUDE SHADING FACTORS $|V_j|$

IV. CONCLUSIONS

A computational procedure has been developed which permits the specification of a discrete velocity amplitude and phase for finite-width transducer elements in the dome-transducer model. Previously it was necessary to assume a continuous velocity distribution at the transducer in analyzing dome-transducer interactions.

A comparison of computed near- and farfield sound pressures indicates that the newer, more realistic transducer boundary specification results in some changes when compared to previous computations with a continuous velocity specification. For cases with and without the dome, the newer specification results in a rather high pressure amplitude on the inactive (rigid) portion of the transducer. This result indicates that there is some interaction among the active transducer elements and the adjacent inactive elements. This effect is shown in Figs. 8 and 9. In the farfield the side lobes are somewhat lower for the discontinuous boundary with and without the dome. (See Figs. 10 and 11.)

The purpose of shading a transducer array is, of course, to improve the directivity of the array. Other factors, however, should be considered in choosing an array shading. Among these are smoothness of the nearfield pressure and source level - decreasing the velocity amplitudes of some of the elements will reduce the power transmitted to the water. The first factor has implications in regard to cavitation and element loading, each of which can affect system performance. The results in Figs. 4-17 illustrate the near- and farfield effects of the dome for several types of element shading.

In regard to smoothness of the nearfield there does not appear to be much difference in the results for the shading factors

used in the computations; the nearfield sound pressure distributions for each type of shading are all nonsmooth with the dome in place. (See Figs. 4, 6, 12, 14, and 16.)

The results presented in Figs. 5, 7, 13, 15, and 17 indicate how shading can be employed to improve the directivity of the transducer and increase side lobe suppression in the farfield. An interesting result shown in these figures is that in cases of extreme shading, for instance Dolph-Tchebyscheff shading shown in Fig 17, the increase in side lobe level due to the dome is more than for cases having lesser amounts of shading. With Dolph-Tchebyscheff shading, the dome results in an increase in side lobe level of approximately 10 dB, while for cosine shading (Fig. 5) the side lobes are increased only about 5 dB. Hence, it appears that dome effects are more pronounced as the degree of shading is increased. It can be concluded that any program aimed at "optimizing" beam patterns by shading the transducer elements should include a consideration of the effects of the dome.

It is not possible at this time to derive in a closed mathematical form an optimum set of element phase and amplitude factors which include a consideration of the dome. However, the techniques described in this memorandum can be used in developing "optimum" element shading including dome effects through an interactive procedure.

V. REFERENCES

1. An Analysis of the Interaction of the Sonar Dome and Transducer During Transmission (U), A Summary Report, TRACOR Document Number 65-188-C, May 17, 1965.

2. Amplitude shading factors derived by the method of Dolph-Tchebyscheff for the AN/SQS-26 are contained in a letter of April 20, 1964, from G. T. Kemp (TRACOR) to R. E. Baline (USL), Ref. NObsr-91039.

3. P. M. Morse, Vibration and Sound, McGraw-Hill, New York, 1948, p. 298.

4. This expression is obtained by differentiating with respect to r the identity

$$e^{ikr\cos\theta} = \sum_{n=0}^{\infty} \epsilon_n i^n J_n(kr)\cos n\theta .$$

See e.g., E. Jahnke and F. Emde, Tables of Functions, Dover, New York, 1945, p. 149.

5. A. E. H. Love, Mathematical Theory of Elasticity, Dover, New York, 1944, p. 544.

6. P. M. Morse and H. Feshbach, Methods of Theoretical Physics. McGraw-Hill, New York, 1953, p. 1371, p. 631.

7. W. Flügge, Stresses in Shells, Springer-Verlag, Berlin, 1960. The equilibrium shell equations of Flügge, page 219, are modified to include acceleration terms.

TRACOR, INC 1701 Guadalupe St Austin, Texas 78701

APPENDIX A

APPENDIX A. THE SOUND PRESSURE FIELD PRODUCED BY A TRANSDUCER RADIATING IN A CONCENTRIC DOME

The mathematical model illustrated in Figure 1 consists of an infinite-length cylinder and concentric shell. A velocity distribution independent of the axial direction is specified on the surface of the cylinder, and it is desired to find the resulting sound pressure field in the fluid in Regions 1 and 2 of Figure 1. The boundary value problem as stated is a three region problem (two fluid regions and the shell). In general partial differential equations must be solved both in the two fluid regions and in the region of the shell material, and boundary conditions must be matched at shell-fluid interfaces as well as at the cylinder-fluid interface. However, the problem is considerably simplified by using the results of elastic shell theory to describe the motion of the shell's middle surface, thus eliminating the necessity of solving the full partial differential equations of linear elasticity for the shell material. Further, since the shell is thin relative to other geometrical parameters, the boundary conditions at shell-fluid interfaces can be matched at the middle surface of the shell.

A. Sound Pressure Field in the Fluid

It is assumed that in Regions 1 and 2 the acoustic pressure p obeys the scalar wave equation[3]

$$\frac{1}{r}\frac{\partial}{\partial r}\left(r\frac{\partial p}{\partial r}\right)+\frac{1}{r^2}\frac{\partial^2 p}{\partial \theta^2}=\frac{1}{c^2}\frac{\partial^2 p}{\partial t^2} \tag{1}$$

where r and θ are the space coordinates, t is the time, and c is the propagation velocity in the fluid.

For a harmonic time dependence the general solution to Eq. 1 is[3]

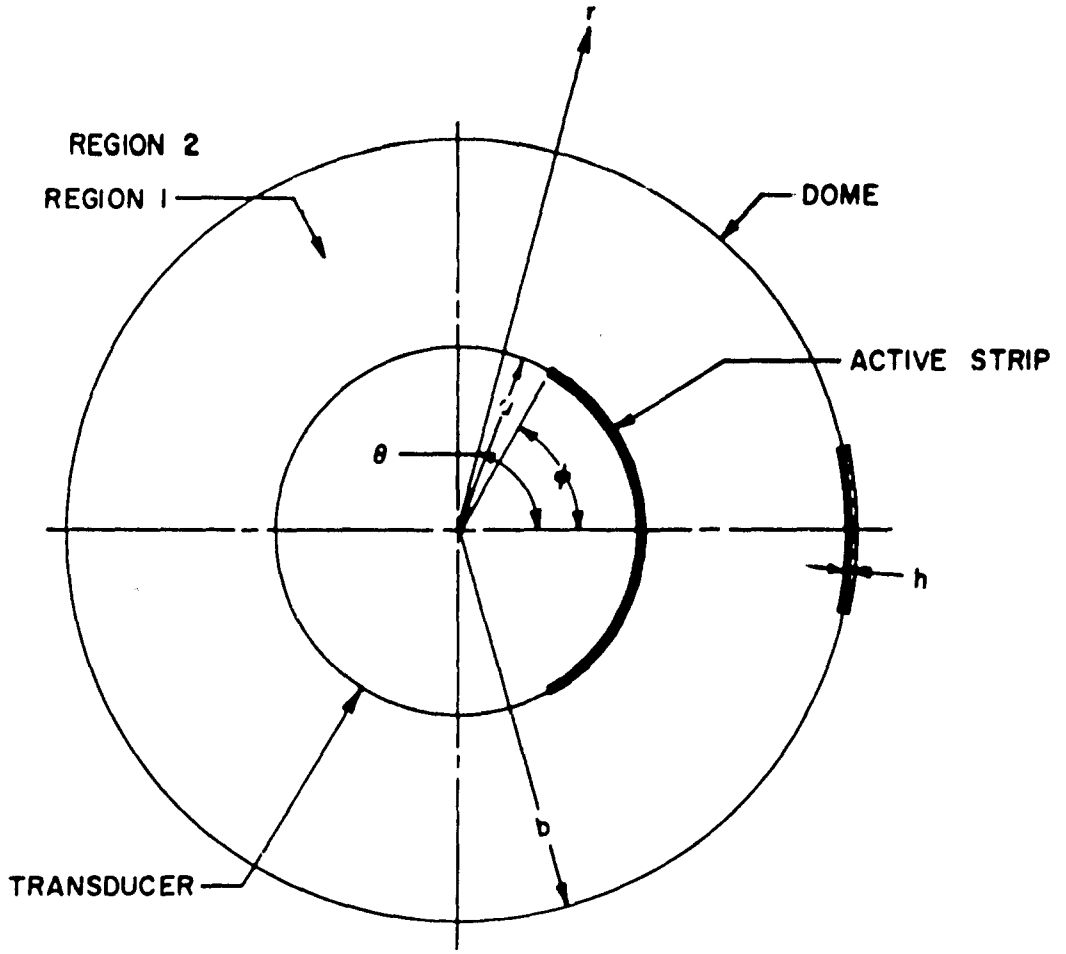

FIG. 1 - GEOMETRY FOR A CYLINDRICAL TRANSDUCER RADIATING IN A CONCENTRIC DOME

TRACOR, AUSTIN, TEXAS
1 DWG. 778-1
3/18/66 BM/LSH

$$p = \sum_{n=0}^{\infty} [A_n H_n^{(1)}(kr) + B_n H_n^{(2)}(kr)] \cos n\theta \, e^{-i\omega t} \qquad (2)$$

where $H_n^{(1)}$ and $H_n^{(2)}$ are the nth order Hankel functions of the first and second kind, respectively, ω is the angular frequency, $k = \omega/c$, and A_n and B_n are constants which will be determined by boundary conditions. Equation 2 involves only cosine terms as it is anticipated that problems to be analyzed will possess symmetry about $\theta=0$. In Region 1 the sound pressure field is*

$$p_1 = \sum_{n=0}^{\infty} [A_n H_n^{(1)}(kr) + B_n H_n^{(2)}(kr)] \cos n\theta \quad . \qquad (3)$$

The sound pressure and the radial component v_r of the fluid velocity, with harmonic time dependence, are related by

$$\frac{-1}{\rho} \frac{\partial p}{\partial r} = \frac{\partial v_r}{\partial t} = -i\omega v_r \qquad (4)$$

At the shell-fluid interfaces this component of the fluid velocity must equal the velocity of the shell. (This restriction does not apply to velocity components tangential to the interface because the fluid is regarded as inviscid and hence will not support shear forces.) Denoting the velocity on the cylinder by V_r and the radial component of the velocity of the shell by w, the interface conditions at r=a and r=b are

$$\frac{1}{i\omega\rho} \left.\frac{\partial p_1}{\partial r}\right|_{r=a} = V_r \qquad (5)$$

$$\frac{1}{i\omega\rho} \left.\frac{\partial p_1}{\partial r}\right|_{r=b} = w \quad . \qquad (6)$$

*The time component $e^{-i\omega t}$ will be suppressed in the following.

In the case of interest, a section of the cylinder of angular extent 2φ is phased to represent a plane velocity distribution of uniform amplitude, while the remainder of the cylinder is rigid. This condition can be written as

$$V_r = \frac{1}{\rho c} \cos\theta \, e^{ika\cos\theta} \quad , \qquad |\theta| < \varphi \ ,$$

$$= 0 \quad , \qquad |\theta| > \varphi \ . \tag{7}$$

A Fourier series for the function $\cos\theta \, e^{ikr\cos\theta}$ may be obtained by differentiating the identity,[4]

$$e^{ikr\cos\theta} = \sum_{n=0}^{\infty} \epsilon_n \, i^n \, J_n(kr) \cos n\theta$$

where $\epsilon_o = 1$, $\epsilon_n = 2$ for $n > o$, and J_n is the Bessel function. Then

$$V_r = \frac{1}{i\rho c} \sum_{n=0}^{\infty} \epsilon_n \, i^n \, J_n'(ka) \cos n\theta \quad , \qquad |\theta| < \varphi \ ,$$

$$= 0 \quad , \qquad |\theta| > \varphi \ , \tag{8}$$

where the prime indicates a derivative with respect to the argument. Equation 8 can be represented by the Fourier series

$$V_r = \frac{1}{i\rho c} \sum_{n=0}^{\infty} \delta_n \cos n\theta \tag{9}$$

where

$$\delta_n = \epsilon_n \sum_{m=0}^{\infty} \epsilon_m \, i^m \, J_m'(ka) \left\{ \begin{matrix} n \\ m \end{matrix} \right\}$$

and

$$\begin{Bmatrix} n \\ m \end{Bmatrix} = \frac{1}{2\pi}\left[\frac{\sin|n+m|\varphi}{|n+m|} + \frac{\sin|n-m|\varphi}{|n-m|}\right], \quad n \neq m \quad ,$$

$$\begin{Bmatrix} n \\ n \end{Bmatrix} = \frac{1}{2\pi}\left[\frac{\sin 2n\varphi}{2n} + \varphi\right], \quad n \neq 0 \quad ; \quad \begin{Bmatrix} o \\ o \end{Bmatrix} = \varphi/\pi \quad .$$

The substitution of Equations 2 and 9 into Eq. 5 results in

$$\frac{k}{i\omega\rho}\sum_{n=0}^{\infty}[A_n H_n^{(1)'}(ka) + B_n H_n^{(2)'}(ka)]\cos n\theta = \frac{1}{i\rho c}\sum_{n=0}^{\infty}\delta_n \cos n\theta. \quad (10)$$

Noting that the cosine functions are linearly independent and that $k/\omega = 1/c$, Eq. 10 implies

$$A_n H_n^{(1)'}(ka) + B_n H_n^{(2)'}(ka) = \delta_n \quad . \quad (11)$$

The radial component of the shell velocity can be represented in the form[5]

$$w = \sum_{n=0}^{\infty} G_n \cos n\theta \quad . \quad (12)$$

The boundary condition given by Eq. 6 then becomes

$$\frac{k}{i\omega\rho}\sum_{n=0}^{\infty}[A_n H_n^{(1)'}(kb) + B_n H_n^{(2)'}(kb)]\cos n\theta = \sum_{n=0}^{\infty} G_r \cos n\theta \quad (13)$$

or

$$A_n H_n^{(1)'}(kb) + B_n H_n^{(2)'}(kb) = ic\rho\, G_n \quad (14)$$

since the cosine functions are linearly independent.

In writing the general solution for the sound pressure p_2 outside the shell it is necessary to account for the fact that, for large r, the pressure field should have the form of an outgoing wave. Since

$$\lim_{r\to\infty} \left\{ e^{-i\omega t} H_n^{(1)}(kr) \right\} = e^{i(kr-\omega t)} \sqrt{2/\pi\, kr}$$

represents an outgoing wave,[6] the proper form for p_2 is

$$p_2 = \sum_{n=0}^{\infty} C_n H_n^{(1)}(kr) \cos n\theta \quad . \tag{15}$$

The interface condition on the velocities of the fluid and shell on the outside surface of the shell will be matched at the middle surface of the shell, as in Eq. 6. Hence

$$\frac{1}{i\omega\rho} \left. \frac{\partial p_2}{\partial r} \right|_{r=b} = w$$

or

$$\frac{k}{i\omega\rho} \sum_{n=0}^{\infty} C_n H_n^{(1)\prime}(kb) \cos n\theta = \sum_{n=0}^{\infty} G_n \cos n\theta, \tag{16}$$

and, noting the linear independence of the cosine functions,

$$C_n H_n^{(1)\prime}(kb) = ic\rho\, G_n \quad . \tag{17}$$

Equations 11, 14, and 17 give three sets conditions on the four sets of unknowns, A_n, B_n, C_n, and G_n. A consideration of the motion of the shell is necessary to obtain the requisite fourth condition.

B. Motion of the Shell

Let the radial and tangential displacements from equilibrium of the middle surface of the shell be denoted by u_r and u_θ, respectively. Flügge's shell equations are[7]

$$\rho_s \frac{\partial^2 u_\theta}{\partial t^2} = \frac{E_s}{b^2}\left[\frac{\partial^2 u_\theta}{\partial \theta^2} + \frac{\partial u_r}{\partial \theta}\right] \tag{18}$$

$$\rho_s \frac{\partial^2 u_r}{\partial t^2} = \frac{p_- - p_+}{h} - \frac{E_s}{b^2}\left[\frac{\partial u_\theta}{\partial \theta} + u_r\right] - \frac{E_s h^2}{12b^4}\left[\frac{\partial^4 u_r}{\partial \theta^4} + 2\frac{\partial^2 u_r}{\partial \theta^2} + u_r\right] \tag{19}$$

where h is the thickness of the shell and b is the radius of its middle surface, ρ_s is the mass density of the shell material and $E_s = E/(1-\nu^2)$, E being Young's modulus and ν Poisson's ratio. p_- and p_+ are the pressures on the inside and outside shell surfaces, respectively, so $p_- = [p_1]_{r=b}$ and $p_+ = [p_2]_{r=b}$. Since w is the radial velocity of the shell,

$$w = \frac{\partial u_r}{\partial t} = -i\omega u_r . \tag{20}$$

The tangential velocity v of a shell element is represented as

$$v = \frac{\partial u_\theta}{\partial t} = -i\omega u_\theta \tag{21}$$

For symmetry about $\theta=0$, the Fourier series representation for v is of the form[5]

$$v = \sum_{n=0}^{\infty} D_n \operatorname{Sin} n\theta \ . \tag{22}$$

The shell Equations 18 and 19 can be differentiated with respect to time to give conditions on u and v.

$$-\omega^2 \rho_s v = \frac{E_s}{b^2}\left[\frac{\partial^2 v}{\partial \theta^2} + \frac{\partial w}{\partial \theta}\right] \tag{23}$$

$$-\omega^2 \rho_s w = -\frac{i\omega}{h}\left[\, p_1\Big|_{r=b} - p_2\Big|_{r=b}\right] - \frac{E_s}{b^2}\left[\frac{\partial v}{\partial \theta} + w\right]$$

$$- \frac{E_s}{12b^4}\left[\frac{\partial^4 w}{\partial \theta^4} + 2\frac{\partial^2 w}{\partial \theta^2} + w\right] . \tag{24}$$

If Equations 4, 16 and the Fourier series for w and v are substituted into Equations 23 and 24 and the linear independence of the trigonometric functions employed, the following conditions are obtained.

$$-i\omega\left[H_n^{(1)}(kb)\, A_n + H_n^{(2)}(kb)\, B_n\right] + i\omega\, H_n^{(1)}(kb)\, C_n - \frac{h\, E_s\, n}{b^2} D_n$$

$$+ h\left\{\omega^2 \rho_s - \frac{E_s}{b^2}\left[1 + \frac{h^2}{12b^2}(n^4 - 2n^2 + 1)\right]\right\} G_n = 0 \tag{25}$$

$$\left\{\omega^2 \rho_s - \frac{E_s}{b^2} n^2\right\} D_n - \frac{E_s}{b^2} n\, G_n = 0 \quad . \tag{26}$$

C. Determination of the Coefficients

Equations 13, 15, 18, 25, and 26 represent a set of simultaneous algebraic equations in the unknowns A_n, B_n, C_n, D_n, and G_n. This set of equations is readily solved to complete the solutions for the sound pressure field in Regions 1 and 2 given by Equations 3 and 15 respectively.

As an example of the form of the coefficients, the solution for the set of coefficients C_n which are associated with p_2 (Eq. 15) is

$$C_n = \frac{\delta_n}{H_n^{1\prime}(ka) + h\,\gamma_n\,H_n^{1\prime}(kb)\,[J_n'(kb)\,N_n'(ka) - N_n'(kb)\,J_n'(ka)]} \qquad (27)$$

where

$$\gamma_n = \frac{\pi b}{2c^2\rho}\left\{\omega^2\rho_s - \frac{E_s}{b^2}\left[1 + \frac{h^2}{12b^2}(n^4 - 2n^2 + 1)\right] - \frac{E_s^2\,n^2}{b^2(b^2\omega^2\rho_s - E_s\,n^2)}\right\} .$$

This form is typical of the remaining coefficients. It is of interest to note that for $h = 0$, the C_n reduce to the coefficients obtained for a transducer radiating without a dome. This limiting case can be compared to the results of Appendix B[1] where the bare transducer is studied independently.

END

DATE

FILMED

9-21-65